Lecture Notes in Control and Information Sciences 236

Anibal T. de Almeida and
Oussama Khatib (Eds)

# Autonomous Robotic Systems

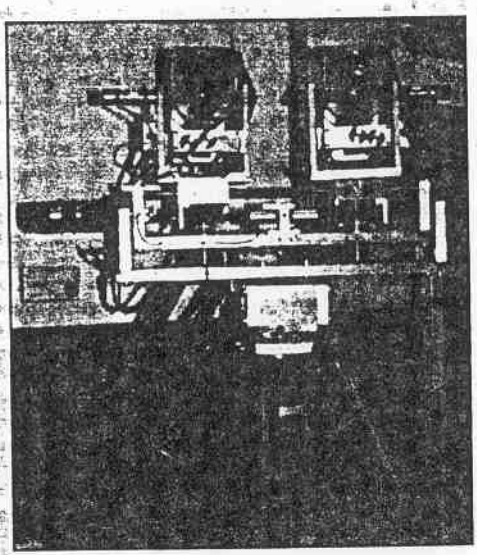

Springer

LNCIS 236 de Almeida and Khatib (Eds) Autonomous Robotic Systems

# LECTURE NOTES IN CONTROL AND INFORMATION SCIENCES



This series aims to report new developments in the fields of control and information sciences – quickly, informally and at a high level. The type of material considered for publication includes:

1. Preliminary drafts of monographs and advanced textbooks
2. Lectures on a new field, or presenting a new angle on a classical field
3. Research reports
4. Reports of meetings, provided they are
   a) of exceptional interest and
   b) devoted to a specific topic.

The timeliness of subject material is very important.

The publication of Lecture Notes is intended as a service to the international scientific and engineering community, in that a commercial publisher, Springer-Verlag, can offer a wider distribution of documents which would otherwise have a restricted readership. Once published and copyrighted, they can be documented in the scientific literature.

**TYPESCRIPTS**

Typescripts should be written in English and be no less than 100, preferably no more than 500, typewritten pages in length, including illustrations. Lecture Notes are printed by photo-offset from printed copy delivered in camera-ready form by the authors/editors. This process does not include a copy editing stage, therefore it is the responsibility of authors/editors to ensure the typescripts are as error-free as possible and printed on a laser or laser quality printer with at least 300 dpi. Careful preparation will help keep production time to the minimum and ensure satisfactory appearance of the finished book.

For best results, text and illustrations in the Camera Ready Copy should fill, but not extend beyond, an area of **120 x 195mm**. Use a 10-point font size with line spacing of 2-points. A traditional serifed typeface (e.g. Times) is preferred. The text should be justified on both left and right margins. Headings should be capitalized and should, with the exception of the title, be aligned to the left. The font sizes preferred are: **Title** – 14pt bold, **2nd level** – 12pt bold, **3rd level** – 10pt bold. Line drawings should be submitted as clear, well-drawn originals, not a sketch or photocopy. They must be positioned on the Camera Ready Copy typescript, centred on the type width. Labelling should not be set smaller than 8pt unless previously agreed with the Springer-Verlag editor. The use of halftone illustrations is, in general, discouraged. However, if such illustrations are considered vital to the work, advance approval from the Springer-Verlag editor is required.

Authors of published monographs receive 30 free copies; editors of published multi-authored works and proceedings receive 20 free copies. Springer-Verlag retains copyright. However, all authors are free to use the material in other publications, with acknowledgment to Springer-Verlag.

Typescripts should be sent to the series editor, Professor Dr.-Ing. M. Thoma, Institut für Regelungstechnik, Technische Universität, Appelstrasse 11, D-30167 Hannover, Germany, or directly to the Engineering Editor, Springer-Verlag London Limited, for review.

Springer-Verlag, Heidelberger Platz 3, D-14197 Berlin, Germany
Springer-Verlag, Tiergartenstrasse 17, D-69121 Heidelberg, Germany
**Springer-Verlag London Ltd, Sweetapple House, Catteshall Road, Godalming, Surrey GU7 3DJ, UK**
Springer-Verlag, 175 Fifth Avenue, New York, NY 10010, USA
Springer-Verlag, 37-3, Hongo 3-chome, Bunkyo-ku, Tokyo 113, Japan

ISBN 1-85233-036-8

9 781852 330361

ISBN 1-85233-036-8

*http://www.springer.co.uk*

## Editors

Professor Anibal T. de Almeida
Instituto de Sistemas e Robótica
Departamento de Engenharia Electrotécnica, Universidade de Coimbra,
Polo II, 3030 Coimbra, Portugal

Professor Oussama Khatib
Department of Computer Science, University of Stanford, Palo Alto, CA 94305,
USA

ISBN 1-85233-036-8 Springer-Verlag Berlin Heidelberg New York

British Library Cataloguing in Publication Data
Autonomous robotic systems. - (Lecture notes in control and
information sciences ; 236)
1.Robotics 2.Automation
I.Almeida, Anibal T. de II.Khatib, O. (Oussama)
629.8'92
ISBN 1852330368

Library of Congress Cataloging-in-Publication Data
A catalog record for this book is available from the Library of Congress



Typesetting: Camera ready by editors
Printed and bound at the Athenæum Press Ltd., Gateshead, Tyne & Wear
69/3830-543210 Printed on acid-free paper

# Sensors for Mobile Robot Navigation

Jorge Lobo, Lino Marques, Jorge Dias, Urbano Nunes, Aníbal T. de Almeida,
Institute of Systems and Robotics
Department of Electrical Engineering
University of Coimbra, 3030 COIMBRA, Portugal
{jlobo, lino, jorge, urbano, adealmeida}@isr.uc.pt

**Abstract:** The article describes a set of sensors relevant for mobile robot navigation. The article describes their sensing principles and includes examples of robust navigation systems for outdoor/indoor autonomous vehicles, applying different low-cost sensors, exploring high integrity and multiple sensorial modalities. There are many applications, from different sectors that could profit from this type of technology: autonomous mobile platforms for materials handling in industry, warehouses, hospitals, etc.; forestry cutting and undergrowth management equipment; autonomous fire-fighting machines; mining machinery; advanced electrical wheel chairs; autonomous cleaning machines; security and surveillance robots. Advanced sensor systems which are now emerging in different activities from the health care services to the transportation sector and domestic services, will significantly increase the capabilities of autonomous vehicles and will enlarge their application potential.

## 1. Introduction to Navigation Systems

The level of automation and complexity of modern society is making evermore demands on the technology. Automation is slowly, but surely, getting to the market place. This includes use of mobile platform for many different purposes like materials handling in industry, floor cleaning, semi-autonomous wheel chairs, semi-automatic de-mining, mining trucks, semi-autonomous cars, etc. As these tasks are being automated, a corresponding set of sensor systems is being developed to enable (semi-) autonomous operation. Navigation, in particular, plays an important role in a great variety of tasks, by allowing autonomous operation to go beyond fixed and structured environments.

Navigation [1] may be defined as the process of directing the movements of a vehicle from one point to another. A remarkable variety of physical principles has been utilised in navigational equipment. Some depend on receipt of information from somewhere outside the vehicle itself, either on or the earth or in the sky. They are therefore subject to error or in-operativeness, when such information is erroneous or is lacking, whether from natural or artificial induced sources [1]. Others are based on internal sensing that is dead-reckoning [2], and do not depend on external references, overcoming some of their associated

[1] The word is derived ultimately from the Latin *navis*, ship, and *agere*, to move or direct.
[2] The origin of the term is "deduced reckoning" from sailing days.



problems, but having others, such as drift. These last systems provide relative position measurements and not absolute positioning. The present location of a vehicle is determined by advancing some previous position through known course and velocity information over a given length of time [2].

Traditional dead-reckoning is not truly self-contained, relying on water speed sensors or wheel encoders that interact with the vehicles environment. Land vehicle dead-reckoning is usually associated with odometry, where encoders are used to measure wheel rotation and steering orientation. What in principle might seem a simple and elegant solution, turns out to be prone to errors, the most common source being wheel-slippage and different or irregular floors. Inertial navigation systems depend on measurements carried out entirely within the vehicle, in accordance with the Newtonian laws of motion and gravitation. Therefore, by relying only on inertial sensor measurements, inertial systems are not affected by the vehicles environment, making them non-jammable and self-contained.

If outdoor mobile robots are to be flexible, they have to navigate in unstructured environments, in which some navigation systems are inoperative or have their performance degraded, but where the self-contained inertial navigation system maintains its performance.

For outdoor vehicles the satellite based Global Positioning System (GPS) is available. The inertial system can provide short-term accurate relative positioning and GPS gives absolute positioning, bounding the error. The deduced reckoning of the inertial system is therefore combined with external reference absolute positioning provided by the GPS.

Range sensors have been also used for mobile robot navigation, and a wide set of applications could be found on [3] and [2]. Their information is very important for collision avoidance, path finding and navigation. Section 6 presents the most common range sensors used on mobile robotics, namely optical range sensors and ultrasonic sensors.

## 2. Inertial Navigation and Inertial Sensors

The principle of generalised relativity of Einstein states that only the specific force on one point and the angular instantaneous velocity, but no other quantity concerning motion and orientation with respect to the rest of the universe, can be measured from physical experiments inside an isolated closed system. Therefore from inertial measurements one can only determine an estimate for linear accelerations and angular velocities. Linear velocity and position, and angular position, can be obtained by integration [4].

Inertial navigation systems implement this process of obtaining velocity and position information from inertial sensor measurements. The basic principle employed in inertial navigation is therefore deduced reckoning. A set of three accelerometers are used to measure acceleration along three orthogonal axes, and their outputs are integrated twice to determine position. To compensate body rotation, three gyroscopes are used to measure rotation rates about three orthogonal axis. In gimballed systems the accelerometers are kept on a gyro-stabilised platform with a high-speed rotor keeping the spatial orientation

constant. In strap-down systems all sensors are rigidly fixed to the vehicle and the gyro data is used to transform the accelerometer data to navigation frame of reference. This can be seen as computationally stabilised accelerometer platforms, as opposed to the physically stabilised platforms used in gimballed systems.

Early versions of INS (Inertial Navigation Systems) were used by the Peenumüde group in Germany, in World War II, to guide the V2 rocket. This was one of the first examples of inertial guidance, relying on a gyro assembly to control the missile's attitude and an integrating accelerometer to sense accelerations along the thrust axis.

INS have since become widespread used in avionics and naval applications. High-grade INS were usually gimballed systems, relying on expensive mechanical components and require high-grade sensors to overcome the severe drift problems due to the double integration of acceleration measurements to determine position. Although the cost of gimballed systems has lowered due to technological developments, it is still rather high for robotic applications.

With new sensor development and more computation power, strap-down systems are becoming more accurate and suitable for high-end applications. They provide high performance and reliability at a lower cost, consume less power and are more compact and lightweight [5].

Recent development in accelerometer and gyroscope technology has lead to some new low-cost sensors, as described in the following section. Strap-down systems based on these low-cost inertial sensors offer performance suitable for mobile robotic applications. The inertial system can be used to provide short-term accurate relative positioning, which combined with some other external reference absolute positioning system, to limit the INS absolute position drift error, will provide a suitable navigation system. Complete INS systems have to consider several factors such as the earth's rotation, and compensate for it in the calculations. But for mobile robotic applications, not travelling long distances along the earth's surface, some simplifications can be made [4].

Gyroscopes and accelerometers are known as inertial sensors since they exploit the property of inertia, i.e. resistance to a change in momentum, to sense angular motion in the case of the gyro, and changes in linear motion in the case of the accelerometer. Inclinometers (also known as clinometers, tilt sensors or level sensors) are also inertial sensors. They measure the orientation of the gravity vector, or to be more exact, the resultant acceleration vector acting upon the sensor. In the following sections we will describe a few of these currently available low-cost sensors.

## 2.1. Accelerometers

A basic accelerometer may be conceived as a basic mass-spring system as shown in figure 1. A proof mass is suspended by an elastic spring (i.e. obeying Hooke's law), the damper is included to control ringing. Upon acceleration of the base frame, the spring must supply a force to make the proof mass keep up, and spring deflection is taken as measure of acceleration. The device is thus a force-measuring instruments which solves the equation



$$F = ma \tag{1}$$

where $m$ is the mass and $a$ acceleration of the sensor, including gravity.

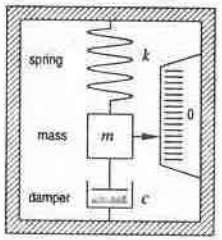


Figure 1. Basic accelerometer.

This damped mass-spring system with applied force constitutes a classical second order mechanical system and the the system's response will depend on the amount of damping. If under-damped, overshoot and oscillation will occur. The system will have the shortest rise time without overshoot when it is critically damped. When the system is over-damped, there will be no overshoot but the rise time will be slow [6].

Practical accelerometers vary in design and technology, but all are based in the equation $F = ma$ in some way. They can be electromagnetic, vibrating string, gyro-pendulum, optical, piezoresistive, piezoelectric, capacitive, amongst others. See [7] and [8] for an overview of some of the older accelerometer technologies.

### *2.1.1. Silicon Accelerometers*

In recent years micro-machined accelerometers have become widely available, largely due to the ability to produce them at low cost. The needs of the automotive industry, namely for airbag deployment systems, encouraged silicon sensor development, enabling the batch-fabrication of the integrated accelerometer sensors. The current commercially available silicon accelerometers incorporate amplification, signal conditioning and temperature compensation. There are presently three main types of micro-machined low cost accelerometers. These are the capacitive, piezoelectric and piezo-resistive types. The piezoelectric sensors have no DC response, making them unsuitable for inertial navigation systems. In the piezo-resistive sensors the acceleration causes a sensing mass to move with respect to a frame, creating stress in a piezo-resistor, which changes its resistor value. The capacitive sensors rely on the displacement of capacitive plates due to the acceleration, creating a mismatch in the capacitive coupling. This change is used to generate a signal proportional to the acceleration applied to the sensor. Some recent devices are open loop sensors, others have a force balancing feedback loop that keeps the sensing element at its central position, gaining improved linearity. These devices are built so as to have a sensing axis and reduced off-axis sensitivity. Some are three-axial, incorporating three ac-

celerometers in one sensor, simplifying mounting and alignment. These sensors present different measurement ranges from $\pm 2\,g$ up to $\pm 500\,g$.

Typical applications of such devices in the automotive industry include frontal impact airbag systems, suspension control, braking control and crash testing. They also find applications in industrial vibration monitoring, transportation shock monitoring and motion control. This large market will push the development of the technology further, and improved performance and lower cost sensors are to be expected.

A silicon accelerometer typically has a silicon spring and a silicon mass. In open loop configurations the acceleration is computed by measuring the displacement of the mass. Typical errors include: non-linearity of the spring; off-axis sensitivity; hysteresis due to the springs or hinges; rotation-induced errors (i.e. when body rotation adds rotational acceleration to the linear acceleration we intend to measure); and accelerometer signal noise.

For higher precision, force balancing closed loop configurations are implemented. Forces are applied to the mass to make it track the frame motion perfectly, and thus zero-balance the mass. Typical restoring forces used in silicon accelerometers include magnetic, piezoelectric and electrostatic. The sensor output will be given by the amount of force necessary to zero-balance the mass. By zero-balancing the mass, errors due to distortions and spring non-linearity are minimised. The input dynamic range and bandwidth is increased. Weaker hinges can be used, reducing hysteresis effects, and mechanical fatigue is minimised. No damping fluid is required, allowing operation in vacuum, and mechanical resonance avoided. Improved precision is thus accomplished.

In order to sense the proof mass displacement, either to directly give the output signal or control the zero-balancing loop, a number of sensing techniques is available. These include piezo-resistive, piezoelectric, capacitive and optical. The piezoelectric accelerometers rely on the deposition of a piezoelectric layer onto the silicon springs. They have a high output at relatively low current, but have high impedance and no DC response. Optical silicon accelerometers rely on the changing characteristics of an optical cavity, due to mass displacement. Radiation penetrating the cavity is band-pass dependent of the mass displacement. This technology has been used in high-resolution, but rather high cost, pressure sensors [9]. Piezo-resistive and capacitive both have DC response and relatively low cost, making them suitable for low-grade inertial navigation systems.

## Piezo-resistive Accelerometers

The first silicon accelerometer prototype was built in 1976 [9]. This device had a single cantilever structure, was fragile and had to be damped with a liquid. Despite its limitations, it represented a significant step from the attachment of silicon strain sensors onto metal diaphragms, to having the resistor diffused onto single-crystal silicon. The basic design structures that have evolved for silicon are shown in figure below 2.

The single cantilever has, in theory, the highest sensitivity, but has more off-axis errors and is rather fragile. The double cantilever provides good off-axis



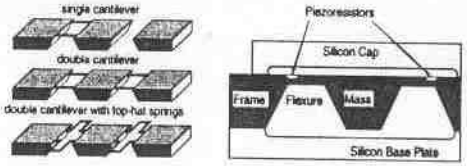


Figure 2. Design structures for the piezo-resistive accelerometer and cross-section of double cantilever sensor (adapted from [10]).

cancellation and is more robust. The folded springs of the top-hat configuration allow for large displacements in a smaller area, thus reducing the cost of the sensor.

## Capacitive Accelerometers

In capacitive accelerometers, proof mass displacement alters the geometry of capacitive sensing elements.

One design of capacitive silicon accelerometers uses a main beam that constitutes the proof mass, with springs at each end. The beam has multiple centre plates at right angles to the main beam that interleave with fixed plates attached to the frame on each side, forming a comb-like symmetric structure. This design allows sensing of positive and negative acceleration along the axis of the main beam in the sensor plane.

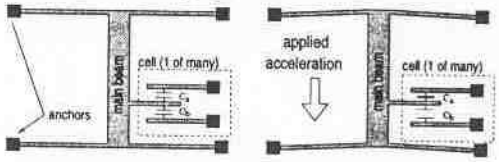


Figure 3. Capacitive comb finger array accelerometer working principle (adapted from [11]).

Each of the centre plates fits between two adjacent fixed plates, forming a capacitive divider, as shown in figure 3. The two fixed plates are driven with an equal amplitude but opposite polarity square wave signals, typically $1\,MHz$.

With no acceleration, the two capacitances are approximately equal and the centre plate will be at approximately zero volts. Any applied acceleration causes a mismatch in plate separation which results in greater capacitive coupling from the nearest fixed plate; a voltage output can thus be detected on the centre plate. The acceleration signal is contained in the phase relative to the driving signal, thus a synchronous demodulator technique is actually used to extract the relatively low frequency acceleration signal.

The resulting acceleration signal is used in a feedback loop to force balance the sensor, impeding the deflection and servoing the sensor back to its $0\,g$ position. The balancing force is obtained electrostatically, caused by driving

the centre plates to a voltage proportional to the acceleration signal. The force-balancing servo loop response has to be fast enough and flat enough to track fast level changes, keeping the sensor nearly motionless, and minimising the errors.

### 2.2. Inclinometers

Though not strictly accelerometers, inclinometers or clinometers, measure the orientation of the resultant acceleration vector acting upon the vehicle. If the vehicle is at rest, this means its orientation with respect to level ground.

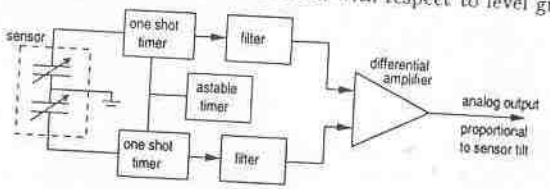


Figure 4. AccuStar inclinometer block diagram.

The concept of the sensor is based on a dielectric fluid, with an air bubble, inside a capacitive sensor. When the sensor is tilted the bubble, moving under the force of gravity, changes the capacitance of the sensor elements. The resulting differential generates an output signal which reflects the relative tilt in the sensing axis as shown in figure 4. Due to the fluids inertia and settling time, and sometimes the measurement method, inclinometers tend to have a delayed response.

The concept of the sensor is based on a dielectric fluid with an air bubble inside a dome shaped capacitive sensor. The sensing dome is divided into four quadrants. When the sensor is tilted, the bubble, moving under the force of gravity, changes the capacitance of the sensor elements in each quadrant. The resulting differential generates an output signal which reflects the relative tilt of the device in either x- or y-axis.

Other designs, still using the principle of the spirit level, measure resistance to obtain the tilt. These sensors have a suitably curved tube, with an electrically conducting liquid and gas bubble inside, and three electrodes. When the sensor is tilted the bubble's position relative to the electrodes changes, causing a difference in the electrical resistance between electrodes proportional to the tilt.

When using inclinometers care should be taken, when accelerations other than gravity are present, since the tilt will be measured relative to the resultant vector. If the sensor is tilted by an angle $\alpha$ to the horizontal and is subject to an acceleration $a$ in a direction normal to the sensor's measuring axis in the horizontal plane, the tilt sensor will not measure $\alpha$. The measured angle will be

$$\alpha_{measured} = \alpha + \tan^{-1}\left(\frac{a}{g}\right) \qquad (2)$$



where $g$ is the modulus of the gravity vector [12].

### 2.3. Gyroscopes

The mechanical gyroscope [3], a well known and reliable but expensive rotation sensor, based on the inertial properties of a rapidly spinning rotor, has been around since the early 1800s. The spinning rotor or flywheel type of gyroscope uses the fundamental characteristic of the angular momentum of the rotor to resist changing its direction to either provide a spatial reference or to measure the rate of angular rotation [5]. Many different designs have been built, and different methods used to suspend the spinning wheel. See [7] for some examples of such devices.

Optical gyroscopes measure angular rate of rotation by sensing the resulting difference in the transit times for laser light waves travelling around a closed path in opposite directions - see figure 5. This time difference is proportional to the input rotation rate, and the effect is known as the 'Sagnac effect', after the French physicist G. Sagnac. Sagnac, in fact, demonstrated that rotation rate could be sensed optically with the Sagnac interferometer as long ago as 1913 [5].

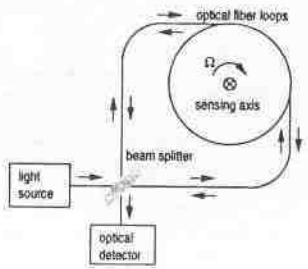


Figure 5. Simplified diagram of optical fibre gyroscope (adapted from [13]).

The communications industry has made optical fibres increasingly available, enabling the construction of low-cost fibre optic gyroscopes. These devices, named FOG or OFG for short, use multiple loops of optical fibre to construct the closed loop path, and semiconductor laser diodes for the light source. A simplified diagram is shown in figure 5. The beam splitter divides the laser beam into two coherent components. The difference of travelling time between the two beams, caused by the difference in optical path lengths, is detected as the interference between the two beams by an optical detector. Several manufactures have produced relatively inexpensive optical fiber gyros for car navigation systems.

But even lower cost, and becoming increasingly compact are the vibrating structure gyroscopes. These use the Coriolis effect whereby an object with linear motion in a rotating frame of reference, relative to inertial space, will experience a so called Coriolis acceleration given by

[3] from the Greek word *gyros* meaning rotation and *skopein* meaning view.

$$\vec{a}_{coriolis} = 2\vec{\varpi} \times \vec{v} \tag{3}$$

where $\vec{\varpi}$ is the angular velocity of the rotating frame and the object's velocity $\vec{v}$ is given in the rotating frame of reference. Imagine a ball rolling across a rotating table. An outside observer would see it moving along a straight line. But an observer on the table would see the ball following a non-linear trajectory, as if a mysterious force was driving it. This apparent force is called the Coriolis force. You can see from equation 3 that the Coriolis force will be perpendicular to both the rotation axis and the objects linear motion.

### 2.3.1. *Vibrating Structure Gyroscopes*

The basic principle of Vibrating Structure Gyroscopes (VSG), is to have radial linear motion and measure the Coriolis effect. If a sensing element is made to vibrate in a certain direction, say along the x-axis, rotating the sensor around the z-axis will produce vibration in the y direction with the same frequency. The amplitude of this vibration is determined by the rotation rate. The geometry used takes into account, amongst other factors, the cancelling out of unwanted accelerations.

The common house fly, in fact, uses a miniature vibrating structure gyro to control its flight. A pair of small stalks with a swelling at their ends constitute radially oscillating masses that will be subject to Coriolis forces when yaw is experienced. These forces will generate muscular signals that assist the acrobatic fly [3].

#### The Vibrating Prism Gyroscope

A piezoelectric vibrating prism sensor can be used for sensing angular velocity. The device' s output is a voltage proportional to the angular velocity. The principle of the sensor is outlined in figure 6. Inside the device there is an equilateral triangle prism made from *elinvar*, elastic invariable metal, which is fixed at two points. Three piezoelectric ceramic elements are attached to the faces of prism, one on each side. The prism is forced to vibrate by two of the piezoelectric elements, whilst the other is used for feedback to the drive oscillator. These two elements are also used for detection. When there is no rotation they detect equally large signals. When the prism is turned, Coriolis forces will affect the prism vibration and the sensing piezoelectric elements will receive different signals. The difference between the signals is processed by the internal analogue circuits to provide an output voltage proportional to the angular velocity [14].

#### The Tuning Fork Gyroscope

A micro-miniature double-ended piezoelectric quartz tuning fork element can be used to sense angular velocity. The sensor element and supporting structure are fabricated chemically from a single wafer of mono-crystalline piezoelectric quartz.

The drive tines, being the active portion of the sensor, are driven by a high frequency oscillator circuit at a precise amplitude, producing the radial



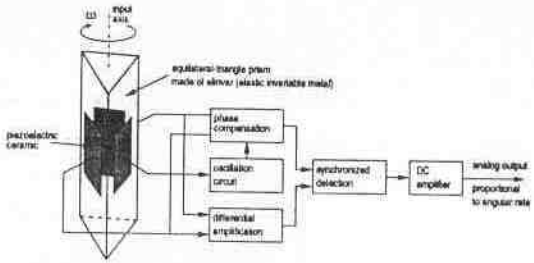


Figure 6. Piezoelectric vibrating prism gyroscope (adapted from [14]).

oscillation of the tines along the sensor plane, as shown in figure 7. A rotational motion about the sensor's longitudinal axis produces a DC voltage proportional to the rate of rotation due to the Coriolis forces acting on the sensing tines. Each tine will have a Coriolis force acting on it of:

$$F = 2m\varpi_i \times V_r \tag{4}$$

where $m$ is the tine mass, $V_r$ the instantaneous radial velocity and $\varpi_i$ the input angular rate. This force is perpendicular to both the input angular rate and the instantaneous radial velocity.

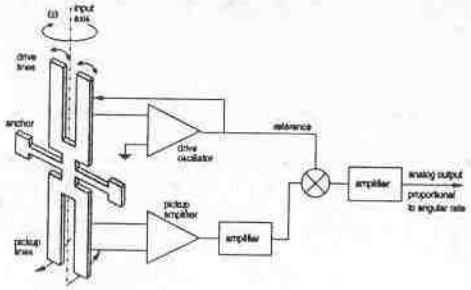


Figure 7. Example of tuning fork gyroscope (adapted from [15]).

The two drive tines move in opposite directions, and the resultant forces are perpendicular to the plane of the fork assembly, and also in opposite directions. This produces a torque which is proportional to the input rotational rate. Since the radial velocity is sinusoidal, the torque produced is also sinusoidal at the same frequency of the drive tines, and in-phase with the radial velocity of the tine.

The pickup tines respond to the oscillating torque by moving in and out of plane, producing a signal at the pickup amplifier. The sensed pickup signal is then synchronously demodulated to produce the output signal proportional to the angular velocity along the sensor input axis.

## 3. Fluxgate Compass

One good source for absolute heading of outdoor mobile robots is the earth's magnetic field. The magnetic compass has long been used in navigation. Mechanical magnetic compasses have evolved from the simple magnetised needle floating in water, to the more sophisticated and time proven systems in use today. Much more practical and suitable for mobile outdoor robots are the fluxgate compasses. These saturable-core magnetometers use a gating action on AC-driven excitation coils to induce a time varying permeability in the sensor core, hence the name fluxgate. Highly permeable materials present a lower magnetic resistance path and will draw in the lines of flux of an external uniform magnetic field. If the material is forced into saturation by an additional magnetising force, the material will no longer affect the lines of flux of the external field. The fluxgate sensor uses this saturation phenomenon by driving the core element into and out of saturation, producing a time varying magnetic flux density that will induce e.m.f. changes in properly oriented sensing coils. These variations will provide a measurement of the external DC magnetic field. See [2] for a more detailed description.

One example of such a device is the C100 model from KVH Industries, Inc. This fluxgate sensor uses a saturable ring core element, free floating in an inert fluid within a cylindrical lexan housing. The lexan housing is surrounded by windings which electrically drive the coil into and out of saturation. Pulses, whose amplitude is proportional to the sensed horizontal component of the earth's magnetic field, are detected by two secondary windings. The secondary windings are at right angles, as can be seen in figure 8, thereby providing data on the x and y horizontal components of the earth's magnetic field.

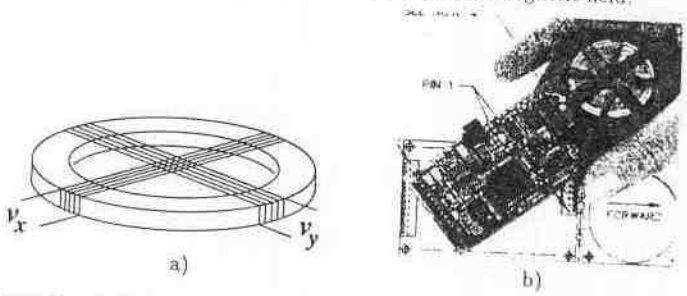


Figure 8. a) Flux-gate sensor element (adapted from [16]); b) KVH-C100 Compass engine (photo adapted from [17])

These signals are then converted to a DC level, digitised and sent to a microprocessor that calculates the azimuth angle as

$$\Phi = \tan^{-1} \frac{v_x}{v_y} \tag{5}$$

The microprocessor also performs compensations based on previous calibrations that substantially increase the sensor's accuracy. Several output modes are available, including a serial RS-232 port to provide heading information and also perform compass configuration.



## 4. Global Positioning System - GPS

### 4.1. Introduction

One of the most relevant external sensors, for outdoor applications, is the Global Positioning System (GPS). Navigation employing GPS and inertial sensors in a synergistic relationship and the integration of these two types of sensors not only overcomes performance issues found in each individual sensor, but could produce a system whose performance exceeds that of the individual the sensors.

The inertial systems accuracy degrades with time, but GPS provides bounded accuracy. GPS and INS complement each other, and their information can be combined to provide an overall better system. The GPS enables calibration and correction of the INS drift errors by means of a Kalman filter. The INS can smooth out the step changes in the GPS position output, which can occur when switching to another satellite or due to other errors.

### 4.2. Overview of the GPS system

The GPS system was designed for, and is operated by, the U. S. military system. Its scope for military missions has been far outgrown with civilian applications, both commercial and scientific. The U. S. Department of Defence funds and controls the system, and civilian users world-wide can use the system free of charge and restrictions. However the accuracy is intentionally degraded for the non-military applications. The satellite-based systems can provide service to an unlimited number of users since the user receivers operate passively (i.e. receive only). The system provides continuous, high accuracy positioning anywhere on the surface of the planet and near space region, 24 hours a day, under all weather conditions. GPS also provides a form of co-ordinated universal time. The users receivers are small and lightweight, making hand-held global positioning systems a reality. See [18] for a brief history and description of the system or [19] for a more detailed description and underlying principles.

The GPS system is composed of three segments. The space segment consists of the GPS operational constellation of satellites. The constellation consists of 24 earth satellites, including 3 active spares, in 12 hour orbits. They are arranged in six orbital planes, separated by 60° in longitude, and inclined at about 55° to the equatorial plane. The satellites' nearly circular orbit, with an altitude of around 20 000 $km$, is such that they repeat exactly twice per sideral day. This implies that they repeat their ground track 4 minutes later each day. This constellation provides the user with between 5 and 8 satellites visible from any point on earth. GPS operation requires a clear line of sight, and since the signals cannot penetrate water, soil, or walls very well, satellite visibility can be affected by those types of obstacles. The control segment consists of a world-wide system of tracking stations. A Master Control Station tracks the position of all satellites and maintains the overall system time standard. The other monitor stations measure signals from the satellites, allowing the Master Sta-

tion to compute the satellites exact orbital parameters (ephemeris) and clock corrections, and upload them to the satellites, at least once a day. The satellite then sends subsets of this information to the user receivers. Satellites have redundant clocks, allowing them to maintain synchronous GPS system time. The user segment consists of the GPS receivers. They convert the satellite signals into position, velocity, and time estimates.

Position measurement is based on the principle of range triangulation. The receiver needs to know the range to the satellites and the positions of these satellites. The satellites positions can be determined by the ephemeris data broadcast from each satellite.

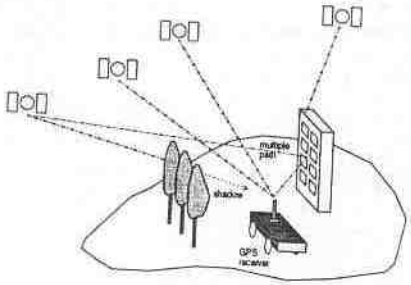


Figure 9. GPS basic idea.

The ranges are determined by measuring the signal propagation time from each satellite to the receiver. The receiver needs a local clock synchronised with the GPS system time. The atomic clock used in the satellites are impractical for the user receivers, and cheap crystal oscillators are used instead. These introduce a user clock bias that effectively adds a fourth unknown in the triangulation. The computed range to each satellite will be equally affected by the same clock bias dependent variable. These erroneous ranges are called pseudo-ranges. To determine position in three dimensions, four equations are needed to determine the four unknowns. For each satellite the following equation holds:

$$pseudorange_{sat_i} = \sqrt{(x - x_{sat_i})^2 + (y - y_{sat_i})^2 + (z - z_{sat_i})^2} + c\Delta t \qquad (6)$$

where receiver and satellite positions are expressed in Cartesian geocentric coordinates, $c$ is a constant, and $\Delta t$ is the user clock bias, which it the same for every satellite, since the satellite clocks are synchronous [20]. Four satellites will be needed, and the three dimensional position will be given by the simultaneous solution(s) of the four equations. This is done in practice with a standard Newton-Raphson method for solving simultaneous non-linear equations. When more satellites are used, or some prior knowledge is available, a least squares technique is used. When altitude is known, navigation in two dimensions can be done with only three satellites.

All satellites broadcast two microwave carrier signals, L1 (1575.42 $MHz$) and L2 (1227.60 $MHz$), as well as UHF intra-satellite communications link, and S-band links to ground stations. The dual frequency approach allows estimation of ionospheric propagation delay at the receiver since the delay is frequency dependent. Satellites use unique Pseudo Random Noise (PRN) codes to modulate the signals, enabling satellite identification at the receiver end. The use of a particular type of PRN codes allows receivers with antenna only a few inches across to extract very low power signals from background noise by correlating them with expectations. The PRN codes of the different satellites are nearly uncorrelated with respect to each other, allowing receivers to "tune in" to different satellites by generating the appropriate PRN code and correlating with the received signal. The receiver computes satellite signal propagation time by shifting the self generated PRN code sequence in time, until the correlation function peaks. The time shift introduced gives the signal propagation time, including clock bias.



### 4.3. GPS errors

Selective Availability (SA) is a deliberate error introduced to degrade system performance for non-U.S. military and government users. The system clocks and ephemeris data is degraded, adding uncertainty to the pseudo-range estimates. Since the SA bias, specific for each satellite, has low frequency terms in excess of a few hours, averaging pseudo-ranges estimates over short periods of time is not effective [21]. The potential accuracy of 30 meters for C/A code receivers is reduced to 100 meters.

Satellites are subject to deviations from their planned ephemeris, introducing ephemeris errors. The satellite clocks degrade over time, and if the ground control leaves then uncorrected, unwanted clock errors are introduced.

The troposphere (sea-level to 50 $km$) introduces propagation errors that are hard to model, unless local atmospheric data are available. The ionosphere (50 $km$ to 5000 $km$) also introduces delays, and some compensation can be made with modelling based on almanac data. Dual frequency receivers allow direct estimation of ionospheric propagation delay since the delay is frequency dependent.

Shadows and multiple paths, as seen in figure 9, can also introduce errors. Shadows reduce the number of visible satellites available for positioning. Multiple path error is caused by reflected signals from surfaces near the receiver and can be difficult to detect and hard to avoid. The reflected signal can either interfere, or be mistaken for, the straight line path signal form the satellite.

### 4.4. Differential GPS (DGPS)

The basic idea behind differential positioning is to correct bias errors at the receiver with measured bias errors at a known nearby position. The reference receiver, knowing the satellites' ephemeris and the expected signal propagation delay, can calculate the corrections for the measured transit times. This correction is computed for each visible satellite signal, and sent to the user receiver. These pseudo-range corrections can be radio broadcast to multiple user receivers. A more simplistic approach would be to simply correct the user position with the known position offset of the reference receiver. But this

would only provide good corrections if both receivers where using the same set of satellites.

Another differential technique is the carrier-phase DGPS, also known as interferometric GPS, which bypasses the pseudo-random code and uses the high resolution carriers. The phase shift between signals received at the base and mobile units gives the signal path difference. It is also called code-less DGPS, as opposed to the coded DGPS where the pseudo-random noise code sequence is used to estimate signal path differences for each satellite. This technique is typically used in surveying applications, where accuracy of a few centimetres can be achieved. Besides the high cost, code-less DGPS requires a long set-up time, is subject to cycle slip, and unsuitable for fast moving vehicles.

## 5. Visual and Inertial Sensing Integration

In human and other animals the ear vestibular system gives inertial information essential for navigation, orientation or equilibrium of the body. In humans this sensorial system is located in the inner ear and it is crucial for several visual tasks and head stabilisation. The human vestibular system appears as a special sensorial modality, that co-operates with other sensorial systems and gives essential information for everyday tasks.

One example of co-operation is between the vestibular sensorial system and the visual system. It is well known that the inertial information plays an important role in some eye and head movements [22].

The information provided by the vestibular system is used during the execution of these movements, as described by Carpenter [22]. However the inertial information is also important for head-stabilisation behaviours, including the control of posture and equilibrium of the body.

The inertial information can also be useful on applications with autonomous systems and artificial vision. In the case of active vision systems, the inertial information gives a second modality of sensing that gives useful information for image stabilisation, control of pursuit movements, or ego-motion determination when the active vision system is used with a mobile platform. This kind of sensorial information is also crucial for the development of tasks with artificial autonomous systems where the notion of horizontal or vertical is important, see Viéville for one example [4].

The inertial system prototype described in this section is used in a mobile robot with an active vision system as illustrated in figure 10. The following sections describe the mobile system used and a first approach of inertial and vision data fusion, namely in identifying the ground plane.

### 5.1. An Inertial System based on Solid-State Devices

To study the integration of the inertial information in artificial autonomous systems that include active vision systems it was decided to develop an inertial system prototype composed of low-cost inertial sensors. Their mechanical mounting and the necessary electronics for processing were also designed. The sensors used in the prototype system include a three-axial accelerometer, three gyroscopes and a dual-axis inclinometer.



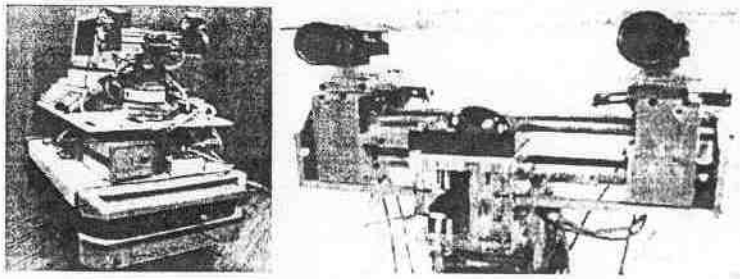

Figure 10. The mobile system with the active vision system. The inertial system prototype was designed to use with this system.

The three-axial accelerometer chosen for the system, while minimising eventual alignment problems, did not add much to the equivalent cost of three separate single-axis sensors. The device used was Summit Instruments' 34103A three-axial capacitive accelerometer. In order to keep track of rotation on the x-, y- and z-axis three gyroscopes were used. The piezoelectric vibrating prism gyroscope Gyrostar ENV-011D built by Murata was chosen. Since orientation is obtained by integration of the angular velocity over time, drift errors will occur. In the prototype, a magnetic flux-gate compass was used to overcome this problem, providing an external reference - see [23] for details. To measure tilt about the x and y-axis a dual axis AccuStar electronic inclinometer, built by Lucas Sensing Systems, was used.

To handle the inertial data acquisition, and also enable some processing, a micro-controller based card was built. This card has analogue filters, an A/D converter as is based on Intel's 80C196KC micro-controller. The robot's master processing unit has an EISA bus interface, where the card is connected along with another for image acquisition and processing. This card is a frame grabber module with two Texas Instruments TMS320C40 DSPs that handles the video processing.

Figure 11 shows the architecture of the system and the computer that supervises the active vision, moving platform and inertial system. The inertial sensors were mounted inside an acrylic cube, enabling the correct alignment of the gyros, inclinometer (mounted on the outside) and accelerometer, as can be seen in the close up of figure 10. This cube is connected to, and continuously monitored by, the micro-controller card in the host computer. The inertial unit is placed at the middle of the stereo camera baseline. The head co-ordinate frame referential, or Cyclop $\{C_y\}$is defined as having the origin at the centre of the baseline of the stereo cameras.

The inclinometer data can be used to determine the orientation of the ground plane. In order to locate this plane in space at least one point belonging to the ground plane must be known. When the vehicle is stationary or subject to approximately constant speed the inclinometer gives the direction of $\vec{g}$ relative to the Cyclop referential $\{C_y\}$. Assuming the ground is levelled,

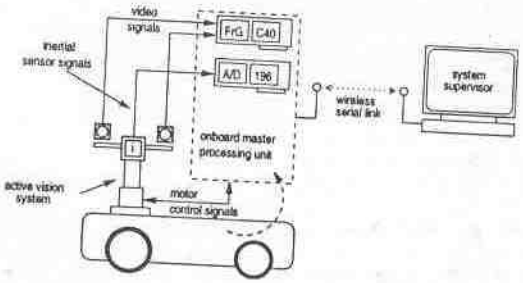


Figure 11. System Architecture. The inertial system processing board uses the Master processing unit as host computer.

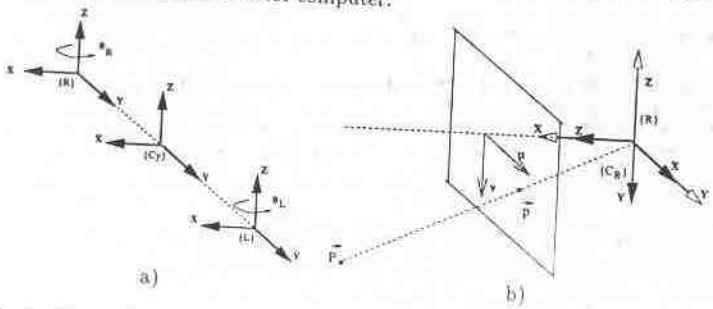


Figure 12. a) System Geometry; b) The camera referential and picture co-ordinates.

and with $\alpha_x$ and $\alpha_y$ being the sensed angles along the $x$ and $y$-axis, the normal to the ground plane will be

$$\hat{n} = -\frac{\vec{g}}{||\vec{g}||} = \frac{1}{\sqrt{1-\sin^2\alpha_x \sin^2\alpha_y}} \begin{bmatrix} -\cos\alpha_x \sin\alpha_y \\ -\cos\alpha_y \sin\alpha_x \\ \cos\alpha_y \cos\alpha_x \end{bmatrix} \quad (7)$$

given in the Cyclop frame of reference. Using this inertial information the equation for the ground plane will be given by

$$\hat{n}.\vec{P}_f + h = 0 \quad (8)$$

where $\vec{P}_f$ is a point in the plane and $h$ is the distance from the origin of $\{C_y\}$ down to the ground plane.

To obtain a point belonging to the ground plane it will be necessary to find the correspondence between points in the image. Establishing this correspondence will give us enough equations to determine the 3D co-ordinates, if a few vision system parameters are known. However if visual fixation is used, the geometry is simple and the reconstruction of the 3D fixated point is simplified,



as can be seen in figure 13. Notice that the visual fixation can be achieved by controlling the active vision system and the process allows a fast and robust 3D reconstruction of the fixation point. This mechanism was developed in the ISR laboratory and is described in [24] and [25]. If the active vision system fixates in a point that belongs to the ground plane, the ground plane could be determined in the Cyclop referential $\{C_y\}$ using the reconstructed point $\vec{P}_f$ and the inclinometer data. Hence, any other correspondent point in the image can be identified as belonging or not to the ground plane.

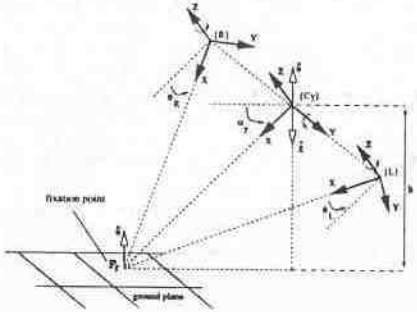


Figure 13. Ground plane point fixated. The point $\vec{P}_f$ in the ground plane is visualised by the active vision system. The geometry of this visualisation corresponds to a state, named visual fixation.

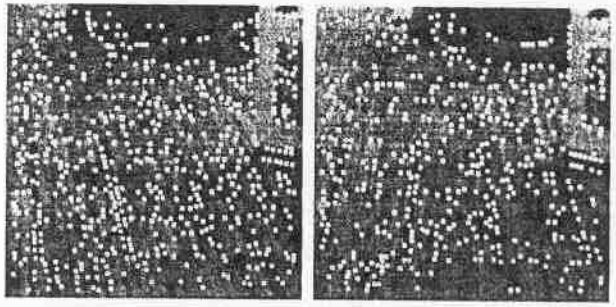

Figure 14. Stereo images with a set of initial points.

Figure 14 shows a pair of stereo images where fixation was obtained for a ground plane point. In this example $\alpha_x$ is null and $\alpha_y = 16.05°$, $\theta = 2.88°$ and $b = 29.6cm$. Making $h = b.\cot(\theta)sin(\alpha_y)/2 \simeq 81,3cm$. The points shown in figure 14 were interest points obtained using SUSAN [26] corner detector. These points are tested by an algorithm that classifies them as belong or not, to the ground plane. Any point in the ground plane verifies a geometric constraint that could between established between two stereo images, easily obtained from

the stereo vision geometry [27]. The ground plane is thus determined. Figure 15 shows the matched ground plane points of interest.

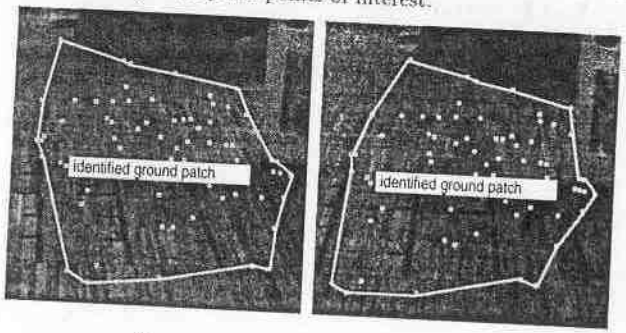


Figure 15. Detected ground points.

## 6. Range Sensors

Range sensors in mobile robots are useful for navigation in unstructured and unknown environments, allowing it to avoid obstacles, detect landmarks or identify navigable routes.

Humans use stereo vision for range sensing and environment perception, but those kinds of techniques are not very adequate for real time control of mobile platforms because they are computing intensive and unreliable.

There are several techniques that can be used for mobile robotics range sensing, namely: magnetic, inductive, capacitive, ultrasound, microwave and optical techniques [3]. Magnetic range sensors can only be used to detect surfaces that generate magnetic fields so its utilization on mobile robotics is very limited. Inductive sensors can be used to measure distance to metallic surfaces, but its range is very short (more or less the diameter of the sensor coil) and its response depends on surface magnetic and conductive properties. On a similar way, capacitive sensors can be used to measure distances up to some centimetres to dielectric surfaces, but its response also depends from the surface dielectric properties.

The most commonly used range sensors in mobile robotics are ultrasound sensors and optical range sensors. Ultrasound sensors are inexpensive and can measure distances up to several meters. Active optical range sensors based on the projection of optical radiation onto a scene can give fast and accurate results. The following section describes the main characteristics of ultrasound sensors and section 6.2 describes the most used optical range sensing methods for mobile robotics.

### 6.1. Ultrasound Sensors

Microwave and ultrasound sensors measure the distance based on the round-trip time of an energy wave between the sensor and a surface. Some ultrasound systems use two transducers, one to transmit and the other to receive the



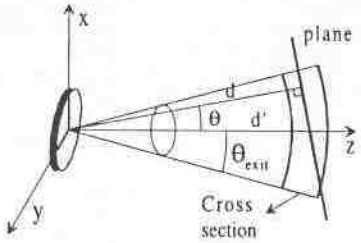


Figure 16. Ultrasonic TOF sensor model.

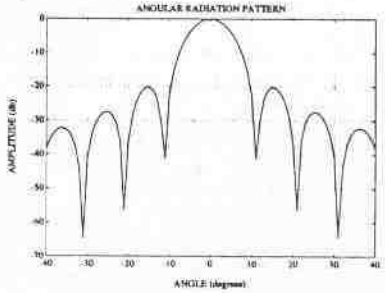


Figure 17. Beam pattern of a Polaroid ultrasonic module.

returned wave.

The propagation velocity ($v$) of an acoustic wave is given by;

$$v = \sqrt{\frac{K_m}{\rho}} \tag{9}$$

where $K_m$ is the modulus of elasticity and $\rho$ is the density of the medium. The relatively low velocity of sound in the air ($331.6 + 0.6 \times {}^{\circ}C\ m/s$), makes possible the ranging with just one transducer that acts both as a transmitter and as a receiver. The transducer emits a short pulse of a longitudinal wave in the ultrasonic spectrum (typically from 20 to 200 $kHz$). If an object intercepts the acoustic field and reflects enough energy to the receiver, the system will provide the range to the object. The maximum detection range depends on the emitted power, on the target cross-sectional area, reflectivity and orientation.

Although these sensors are very independent from surface characteristics, they are affected by the conditions of the propagating medium, namely temperature and humidity. These sensors are very linear, but they have some uncertainty that comes from the Time-Of-Flight (TOF) model. This model predicts that an echo comes from a curved shape volume, so that there will be uncertainty related to the divergence angle, both in depth and in orientation

(see Figure 16). The divergence angle is a function of the transducer radius and resonant frequency, the larger the radius and the frequency, the narrow the divergence angle.

The most popular ultrasonic ranging systems are the Polaroid modules. These modules measure distances from 15 *cm* to about 10 *m* and have an angular beam width of about 12 degrees (see Figure 17). Because ultrasound sensors use acoustic waves, they suffer from low spatial resolution, crosstalk, depth uncertainty, errors due to multiple specular reflections, and low acquisition rates. In spite of these problems, their low cost and easy interface makes them some of the most used range sensors for indoors mobile robotics. Outdoor environments pose some additional problems like noise sources, dust and moisture.

## 6.2. Optical Range Sensors

Optical range sensors are particularly attractive for mobile robotics because they offer real-time accurate measurements with very high spatial resolution. These good properties are possible through the use of good quality optical components, namely coherent light sources (e.g. laser diodes) and very sensitive and high-resolution optical detectors (e.g. CCD cameras and avalanche photodiodes).

This section presents some of the most used optical range sensing methods in robotics, namely intensity reflection, triangulation, telemetry and lens focusing. Complementing surveys on optical range sensors can be found in the references [28, 3, 29, 30].

### *6.2.1. Reflective*

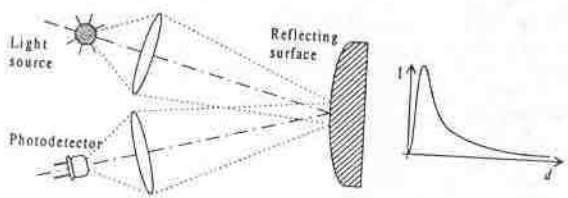


Figure 18. Reflective sensor principle. Some of the light emitted by the source is reflected on the surface and captured by the photodetector. The amount of captured optical light ($I$) depends on the distance ($d$) between the surface and the system.

Return signal intensity sensors are composed by a light emitter and a photodetector whose optical axes can be parallel for long range detection or convergent for shorter range detection (see Figure 18). These sensors measure the distance to an object by the amplitude of light reflected from its surface. The amount of detected light reflected from the object surface can be expressed by the following equation:



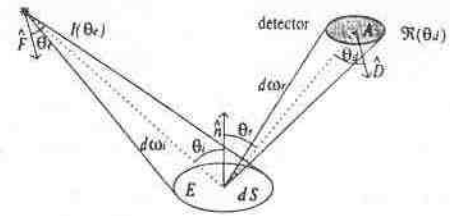


Figure 19. Reflection geometry used to calculate the detected intensity relative to an incremental surface patch.

$$\Phi = \int_S d\phi_r \tag{10}$$

where $d\phi_r$ represents the flux received from an incremental object surface patch (see Figure 19). This flux can be expressed by:

$$d\phi_r = I(\theta_e) \cdot d\omega_i \cdot R \cdot d\omega_r \cdot \Re(\theta_d) \tag{11}$$

where $I(\theta_e)$ is the emitted intensity of light from the solid angle $d\omega_i$, $R$ is the function that characterises the reflectivity pattern of the surface, and $\Re(\theta_d)$ represents the acceptance of the photodetector at an off-axis angle $\theta_d$. All common surfaces have a specular and a lambertian reflective component, so that using a simple model, like Phong's model, the following expression for the surface reflectivity can be obtained [31]:

$$R = K_s.\delta(\theta_r - \theta_i) + K_d.\cos(\theta_r) \tag{12}$$

where $K_s$ and $K_d$ are the coefficients for the specular and lambertian components respectively.

For a sensor with parallel emitter and detector optical axes, the detected intensity varies approximately with the bi-quadratic inverse of the distance [32]. Because the reflected intensity depends heavily from the surface optical characteristics and from its orientation, these sensors suffer from low repeatability. The most commonly found commercial devices are not intended to be used as full range measuring devices, but as simple non-contact presence detectors.

Several manufacturers (e.g. SunX, Banner, Honeywell) provide photoelectric detectors that detect surfaces up to about 1 meter. A common strategy to eliminate the influence of background light, is the utilization of modulated infrared energy and the appropriated optical and electrical filters.

Reflective sensors can be easily homebuilt with increased functionality around a LED and a photodiode. For example some researchers use the IR proximity system to establish data links between a community of mobile robots.

Some mobile robots use IR proximity sensors for short range, narrow beam sensing, together with ultrasound range sensors for medium range, wide beam

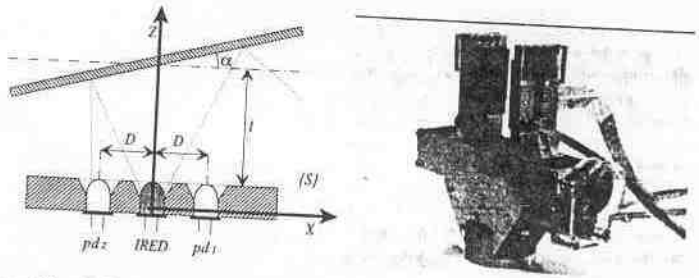


Figure 20. a) Geometry and elements of the proximity sensor. In the picture, $pd_x$ is photo-detector $x$ and $IRED$ is infrared light emitting diode. $S$ represents the co-ordinated system associated to the sensor. b) *Gripper* with a reflective sensor on the extremity of each finger.

sensing. The fusion of both kinds of information improves the results [33, 34] obtained with just one type of sensor.

2-D Reflective Sensor

The ISR Reflex sensor is a small reflective sensor designed to be used on a parallel jaw electrical gripper. This sensor is composed by two photodiodes on opposite sides of a light emitting diode (see Figure 20a). This configuration allows measuring the orientation to a planar homogeneous surface by the difference between the detected intensities in the two photodiodes.

A more detailed description and the sensor modelling can be reached in [32].

Two prototypes of this sensor were integrated on a parallel jaw gripper presented in Figure 20b) for object detection and pre-prehension gripper control. The presence of objects between the gripper fingers is detected by occlusion between the emitter of a finger and the two detectors of the other finger. With this sensorial information, the gripper can align we the object to be grasped and made a smooth transition between position control and contact force control.

When used with planar homogeneous calibrated surfaces, the sensor can measure distances with an accuracy of 0.1 $mm$ on a range from 5 to 100 $mm$. The orientation accuracy is about 0.1°.

A cooperative array of emitters and detectors around a mobile platform can be used in order to estimate surface orientation and profiles based on the several detected intensities. This kind of sensor can help for example on docking tasks.

### 6.2.2. Telemetry

Laser radar sensors or laser range-finders measure the distance $d$ between the sensor and a target surface based on the round-trip time $\Delta t$ of a laser beam (see Figure 21). Considering $v$ the velocity of the propagated wave on the medium, the distance $d$ can be calculated by the following formula:



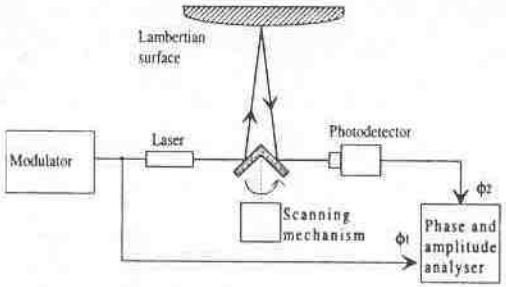


Figure 21. Laser radar. The distance is proportional to the round-trip time of a light pulse between the measuring system and a target surface.

$$2d = v \cdot \Delta t \tag{13}$$

Although these sensors can use three different methods: pulse based time-of-flight (TOF), amplitude modulated (AMCW) and frequency modulated (FMCW), the first two are the most common ones. Pulsed rangefinders emit a short pulse of light and count the time to receive the reflected signal whilst AMCW range finders send an amplitude modulated continuous wave and use the phase shift between the emitted and the received wave to calculate the distance. Range accuracy of AMCW sensors depends upon the modulation wavelength and the accuracy with which the phase shift is measured. For round-trip distances longer than the modulation wavelength there will be ambiguity on the phase shift measurement.

Laser range-finders can measure not only the distance but also the amplitude of the reflected signal (intensity). The fusion of range and intensity images provided by scanning systems, can be helpful for image recognition tasks. These systems are fast, linear and very accurate over a long range of distances, but they are also the most expensive range sensors [35, 36, 37]. Table 1 presents the main characteristics of some currently available scanning systems [38, 39].

### 6.2.3. Triangulation

Triangulation sensors are based on the following trigonometric principle: *if the length of one side along with two interior angles of a triangle are known, then we can determine the length of the two remaining sides along with the other angle.*

An optical triangulation system can be either passive (use only the ambient light of the scene) or active (use an energy source to illuminate the target). Passive triangulation or stereoscopic systems use two cameras oriented to the same scene. The lens central points of each camera along with each point on the scene, define triangles with a fixed baseline (the distance between the central point of each camera lens) and variable interior angles. If the focal distance of each camera is known, these two interior angles can be calculated by the

| Manufacturer | Model | Modulation | field of view | pixels | Accuracy | Min. dist. | Max. distance |
|---|---|---|---|---|---|---|---|
| Acuity Res. | AccuRange 4000 | – | 360°/line | 2000 | 2.5mm | 0 | 50 *feet* |
| ALST[a] | ELRF-3-M | Pulsed/1*Hz* | – | 1 | 2 *m* | 50 *m* | 30 *km* |
| ERIM | Adaptive Suspension | AMCW/14*MHz* | 80° *Az* 60° *El* | 128 × 128 | 3.9 *cm* | – | 19.5 *m* |
| ERIM | Autonomous Land | AMCW/7*MHz* | 80° *Az* 30° *El* | 256 × 64 | 7.8 *cm* | – | 39 *m* |
| ERIM | Intelligent Task | AMCW/720*MHz* | 38° *Az* 38° *El* | 256 × 256 | 2.5 *mm* | – | 0.91 *m* |
| HDOS | US Postal Service | AMCW/700*MHz* | 35° *Az* 35° *El* | 300 × 300 | 0.05 *mm* | – | 1 *m* |
| IMRA | Imaging Laser Radar | AMCW/15*MHz* | 80° *Az* 60° *El* | ~ 3000 | 0.15 *m* | – | 460 *m* |
| Leica | Laser Radar Sensor | – | 90° /line | 128 | < 1 *m* | – | 25 *m* |
| Odetics | ODIN | – | 6° *sr* | – | 0.1 *m* | – | 150 *m* |
| Perceptron | GMS | AMCW/16*MHz* | 60° *Az* 60° *El* | 128 × 128 | 18 *mm* | – | > 10 *m* |
| Riegl | LASAR | AMCW/varies | 60° *Az* 60° *El* | 1024 × 1024 | 2 *mm* | – | 2-40 *m* |
| Riegl | LRI 20x5 | Pulsed | 5° *Az* 20° *El* | 10.000 | ±3 *cm* | 2 *m* | 80 *m* |
| Riegl | LMS-Q140-80 | Pulsed/12*kHz* | 80°/line | 400 | ±2.5 *cm* | 2 *m* | 350 *m* |
| Sandia | LD90-3300 | Pulsed | – | 1 | ±5 *cm* | 3 *m* | 400 *m* |
| Schwartz EO | Scannerless R. Imager | AMCW/5.5*MHz* | ajustable | 256 × 256 | 0.3 *m* | – | varies |
| Schwartz EO | LRF-200 | Pulsed | 360°/line | – | ±30 *cm* | 1 *m* | 100 *m* |
| Schwartz EO | LADAR | Pulsed/9*KHz* | 4° *Az* 10° *El* | 25 × 65 | 0.3 *m* | – | 500 *m* |
| Schwartz EO | Treesense | Pulsed/18*KHz* | 2 × 90° | – | 3 *in* | – | 100 *feet* |
| Sick Optic | Autosense II | Pulsed/15*KHz* | 10° *Az* 30° *El* | 30/line | 3 *in* | 2 *feet* | 50 *feet* |
| | PLS100 | – | 180°/line | | 7 *cm* | – | 50 *m* |

Table 1. Main characteristics of some commercial laser rangefinders.

[a]Very long range. Used normally on military applications.






Figure 22. Triangulation system based on a laser beam and some kind of an imaging camera.

position of each point on both images. The main problem of these systems is due to the identification of corresponding points on both images (feature matching). To obtain a solution for this problem, active triangulation systems replace the second camera by a light source that projects a pattern of light on to the scene. The simplest case of such a sensor, like the one represented in Figure 22, use a laser beam and a one-dimensional camera. The distance ($L$) between the sensor and the surface can be measured by the image position ($u$) of the bright spot formed on the intersection point ($P$) between the laser beam and the surface.

$$L = \frac{B}{tan(\alpha - \gamma)} \tag{14}$$

Where $B$ is the distance between the central point of the lens and the laser beam (baseline) and $\alpha$ is the angle between the camera optical axis and the laser beam. The angle $\gamma$ is the only unknown value in the equation, but it can be calculated using the position ($u$) of the imaged spot (provided that the value of the focal distance $f$ is known).

$$\gamma = \arctan\left(\frac{u}{f}\right) \tag{15}$$

If it is required to obtain a range image of a scene, the laser beam can be scanned or one of several techniques based on the projection of structured light patterns, like light strips [40], grids [41, 42, 43, 44], binary coded patterns [45, 46], color coded stripes [47, 48, 49], or random textures [50] can be used. Although these techniques improve the performance of the range imaging system, they may also present some ambiguity problems [51, 52].

Triangulation systems present a good price/performance relation, they are pretty accurate and can measure distances up to several meters. The accuracy of these systems falls with the distance, but usually this is not a great problem on mobile robotics because high accuracy is only required close to the objects,

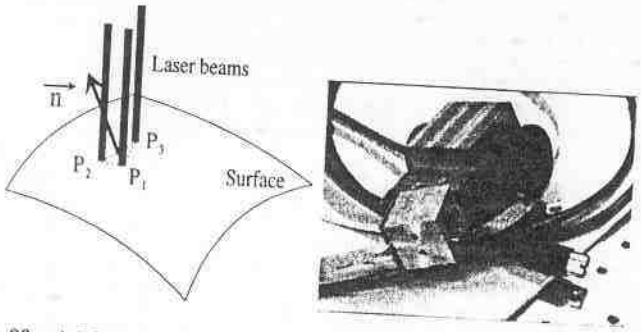


Figure 23. a) Distance and orientation measuring with three laser beams and a Position Sensitive Detector. b) Prototype of the Opto3D measuring head.

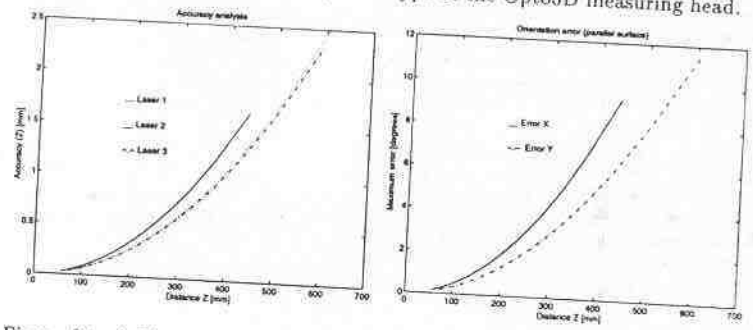


Figure 24. a) Distance accuracy vs. range. b) Angular accuracy for a perpendicular surface.

otherwise it is enough to detect its presence. The main problems of triangulation systems are the possibility of occlusion, and measures on specular surfaces that can blind the sensor or give rise to wrong measures because of multiple reflections [53, 54, 55, 56, 57, 58].

Opto3D

The Opto3D system is a triangulation sensor that uses a PSD[4] camera and three laser beams. Measuring the coordinates of the three intersection points $P_1$, $P_2$ and $P_3$ (see Figure 23a), the sensor can calculate the orientation $\vec{n}$ of the surface by the following expression:

$$\vec{n} = \vec{P_1P_2} \times \vec{P_1P_3} \tag{16}$$

The Opto3D sensor can measure distances up to 75 *cm* with accuracies from 0.05 to 2 *mm* (see Figure 24) [54, 53]. Like every triangulation sensor, the

[4]Position Sensitive Detector



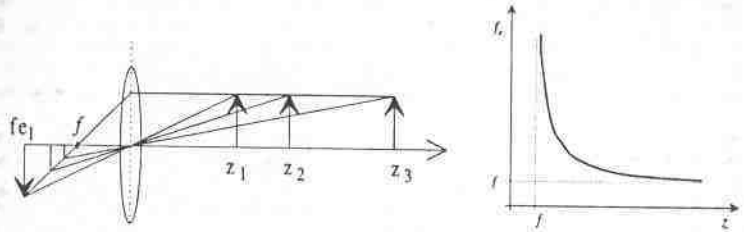


Figure 25. Using the Gauss lens law, it is possible to extract range information from the effective focal distance of an image.

accuracy degrades with the distance. This sensor can measure orientation on a broad range with an accuracy better than 0.1°, and the maximum orientation depends on the reflective properties of the surface (usually only a little amount of light can be detected from light beams that follow over almost tangential surfaces).

### *6.2.4. Lens Focusing*

Focus range sensing relies on Gauss thin lens law (equation 17). If the focal distance ($f$) of a lens and the actual distance between the focused image plane and the lens center ($f_e$) is known, the distance ($z$) between the lens and the imaged object can be calculated using the following equation:

$$\frac{1}{f_e} = \frac{1}{f} - \frac{1}{z} \tag{17}$$

The main techniques exploring this law are **range from focus** (adjust the focal distance $f_e$ till the image is on best focus) and **range from defocus** (determine range from image blur).

These techniques require high frequency textures, otherwise a focused image will look similar to a defocused one. To have some accuracy, it is fundamental to have very precise mathematical models of the image formation process and very precise imaging systems [59].

Image blurring can be caused by the image process or by the scene itself, so depth from defocus technique, requires the processing of at least two images of an object (which may or may not be focused) acquired with different but known camera parameters to determine the depth. A recent system provides the required high-frequency texture projecting an illumination pattern via the same optical path used to acquire the images. This system provide real-time (30 $Hz$) depth images ($512 \times 480$) with an accuracy of approximately 0.2% [60].

The accuracy of focus range systems is usually worse than stereoscopic ones. Depth from focus systems have a typical accuracy of 1/1000 and depth from defocus systems 1/200 [59]. The main advantage these methods is the lack of correspondence problem (feature matching).

## 7. Conclusions

The article described several sensor technologies, which allow an improved estimation of the robot position as well as measurements about the robot surroundings by range sensing. Navigation plays an important role in all mobile robot activities and tasks. The integration of inertial systems with other sensors in autonomous systems opens a new field for the development of a substantial number of applications. Range sensors make possible to reconstruct the structure of the environment, avoid static and dynamic obstacles, build maps and find landmarks.

## References


[1] Altschuler M, et al. 1962 Introduction. In: Pitman G R (ed), *Inertial Guidance*, John Wiley & Sons, pp 1–15

[2] Feng L, Borenstein J, Everett H December 1994 Where am I? - Sensors and Methods for Autonomous Mobile Robot Positioning. Tech. Rep. UM-MEAM-94-21, University of Michigan

[3] Everett H 1995 *Sensors for Mobile Robotics*. A.K. Peters, ISBN 1-56881-048-2

[4] Viéville T, Faugeras O 1989 Computation of Inertial Information on a Robot. In: Miura H, Arimoto S (eds), *Fifth International Symposium on Robotics Research*, MIT-Press, pp 57–65

[5] Collinson R 1996 *Introduction to Avionics*. Chapman & Hall, ISBN 0-412-48250-9

[6] Ausman J S 1962 *Theory of Inertial Sensing Devices*, George R. Pitman (ed.), John Wiley & Sons, pp 72–91

[7] Slater J M 1962 *Principles of Operation of Inertial Sensing Devices*, George R. Pitman (ed.), John Wiley & Sons, pp 47–71

[8] Kuritsky M M, Goldstein M S 1990 *Inertial Navigation*, T. Lozano-Perez (ed), Springer-Verlag New York, pp 96–116

[9] Allen H V, Terry S C, Knutti J W September 1989 Understanding Silicon Accelerometers. *Sensors*

[10] ICSensors January 1988 *Silicon Accelerometers*. Technical Note TN-008

[11] Summit Instruments September 1994 *34100A Theory of Operation*. Technical Note 402

[12] Barshan B, Durrant-Whyte H June 1995 Inertial Navigation Systems for Mobile Robots. *IEEE Transactions on Robotics and Automation*, 11:328–342

[13] Komoriya K, Oyama E 1994 Position Estimation of a Mobile Robot Using Optical Fiber Gyroscope (OFG). In: *Proceedings of the 1994 IEEE International Conference on Intelligent Robots and Systems*, pp 143–149

[14] Murata 1991 *Piezoelectric Vibrating Gyroscope GYROSTAR*. Cat. No. S34E-1

[15] Systron Donner Inertial Division 1995 *GyroChip*. Product Literature

[16] Peters T May 1986 Automobile Navigation Using a Magnetic Flux-Gate Compass. *IEEE Transactions on Vehicular Technology*, 35:41–47

[17] KVH Industries, Inc May 1993 *C100 Compass Engine Technical Manual*. Revision g edn., KVH Part No. 54-0044

[18] Getting I A December 1993 The Global Positioning System. *IEEE Spectrum*, pp 236–247

[19] Kaplan E D 1996 *Understanding GPS: Principles and Applications*. Artech House, ISBN 0-89006-793-7





[20] Kelly A May 1994 Modern Inertial and Satellite Navigation Systems. Tech. Rep. CMU-RI-TR-94-15, Carnegie Mellon University

[21] Dana P H 1997 Global Positioning System Overview. Tech. Rep. CMU-RI-TR-94-15, Department of Geography, University of Texas at Austin, http://www.utexas.edu/depts/grg/gcraft/notes/gps/gps.html

[22] Carpenter H 1988 *Movements of the Eyes*. London Pion Limited, 2nd edn., ISBN 0-85086-109-8

[23] Lobo J, Lucas P, Dias J, de Almeida A T July 1995 Inertial Navigation System for Mobile Land Vehicles. In: *Proceedings of the 1995 IEEE International Symposium on Industrial Electronics*, Athens, Greece, pp 843–848

[24] Dias J, Paredes C, Fonseca I, de Almeida A T 1995 Simulating Pursuit with Machines. In: *Proceedings of the 1995 IEEE Conference on Robotics and Automation*, Japan, pp 472–477

[25] Paredes C, Dias J, de Almeida A T September 1996 Detecting Movements Using Fixation. In: *Proceedings of the 2nd Portuguese Conference on Automation and Control*, Oporto, Portugal, pp 741–746

[26] Smith S, Brady J May 1997 SUSAN - a new approach to low level image processing. *Int Journal of Computer Vision*, pp 45–78

[27] Silva A, Menezes P, Dias J 1997 Avoiding Obstacles Using a Connectionist Network. In: *Proceedings of the 1997 IEEE International Conference on Intelligent Robots and Systems (IROS'97)*, pp 1236–1242

[28] Besl P 1988 Active Optical Range Imaging Sensors. *Machine Vision and Applications*, 1:127–152

[29] Jarvis R March 1983 A perspective on Range Finding Techniques for Computer Vision. *IEEE Trans Pattern Analysis and Machine Intelligence*, PAMI-5:122–139

[30] Volpe R, Ivlev R 1994 A Survey and Experimental Evaluation of Proximity Sensors for Space Robotics. In: *Proc. IEEE Conf. on Robotics and Automation*, pp 3466–3473

[31] Phong B June 1975 Illumination for computer generated pictures. *Commun of the ACM*, 18:311–317

[32] Marques L, Castro D, Nunes U, de Almeida A 1996 Optoelectronic Proximity Sensor for Robotics Applications. In: *Proc. IEEE 8'th Mediterranean Electrotechnical Conf.*, pp 1351–1354

[33] Flynn A 1985 Redundant Sensors for Mobile Robot Navigation. Tech. Rep. 859, MIT Artificial Intelligence Laboratory

[34] Flynn A December 1988 Combining Sonar and Infrared Sensors for Mobile Robot Navigation. *International Journal of Robotics Research*, 7:5–14

[35] Duda R, Nitzan D, Barret P July 1979 Use of Range and Reflectance Data to Find Planar Surface Regions. *IEEE Trans Pattern Analysis and Machine Intelligence*, PAMI-1:259–271

[36] Nitzan D, Brain A, Duda R February 1977 The Measurement and Use of Registered Reflectance and Range Data in Scene Analysis. *Proceedings of the IEEE*, 65:206–220

[37] Jarvis R September 1983 A Laser Time-of-Flight Range Scanner for Robotic Vision. *IEEE Trans Pattern Analysis and Machine Intelligence*, PAMI-5:505–512

[38] Carmer D, Peterson L February 1996 Laser Radar in Robotics. *Proceedings of the IEEE*, 84:299–320

[39] Conrad D, Sampson R 1990 3D Range Imaging Sensors. In: Henderson T (ed), *Traditional and Non-Traditional Robotic Sensors*, Springer-Verlag, Berlin, vol. F63 of *NATO ASI Series*, pp 35–48

[40] Will P, Pennington K June 1972 Grid Coding: A Novel Technique for Image Processing. *Proceedings of the IEEE*, 60:669–680

[41] Stockman G, Chen S, Hu G, Shrikhande N June 1988 Sensing and Recognition of Rigid Objects Using Structured Light. *IEEE Control Systems Magazine*, 8:14–22

[42] Dunn S, Keizer R, Yu J November 1989 Measuring the Area and Volume of the Human Body with Structured Light. *IEEE Trans Systems Man and Cybernetics*, SMC-19:1350–1364

[43] Wang Y, Mitiche A, Aggarwal J January 1987 Computation of Surface Orientation and Structure of Objects Using Grid Coding. *IEEE Trans Pattern Analysis and Machine Intelligence*, PAMI-9:129–137

[44] Wang Y January 1991 Characterizing Three-Dimensional Surface Structures from Visual Images. *IEEE Trans Pattern Analysis and Machine Intelligence*, PAMI-13:52–60

[45] Altschuler M, et al. 1987 Robot Vision by Encoded Light Beams. In: Kanade T (ed), *Three-dimensional machine vision*, Kluwer Academic Publishers, Boston, pp 97–149

[46] Vuylsteke P, Oosterlinck A Feb 1990 Range Image Acquisitionwith a Single Binary-Encoded Light Pattern. *IEEE Trans Pattern Analysis and Machine Intelligence*, PAMI-12:148–164

[47] Kak A, Boyer K, Safranek R, Yang H 1986 Knowledge-Based Stereo and Structured Light for 3-D Robot Vision. In: Rosenfeld A (ed), *Techniques for 3-D Machine Perception*, Elsevier Science Publishers, pp 185–218

[48] Boyer K, Kak A January 1987 Color-Encoded Structured Light for Rapid Active Ranging. *IEEE Trans Pattern Analysis and Machine Intelligence*, PAMI-9:14–28

[49] Wust C, Capson D 1991 Surface Profile Measurement Using Color Frinje Projection. *Machine Vision and Applications*, 4:193–203

[50] Maruyama, Abe S Jun 1993 Range Sensing by Projecting Multiple Slits with Random Cuts. *IEEE Trans Pattern Analysis and Machine Intelligence*, PAMI-15:647–651

[51] Vuylsteke P, Price C, Oosterlinck A 1990 Image Sensors for Real-Time 3D Acquisition: Part 1. In: Henderson T (ed), *Traditional and Non-Traditional Robotic Sensors*, Springer-Verlag, Berlin, vol. F63 of *NATO ASI Series*, pp 187–210

[52] Mouaddib E, Battle J, Salvi J 1997 Recent Progress in Structured Light in order to Solve the Correspondence Problem in Stereo Vision. In: *Proc. IEEE Conf. on Robotics and Automation*, pp 130–136

[53] Marques L 1997 Desenvolvimento de Sensores Optoelectrónicos para Aplicações de Robótica. Master's thesis, DEE, FCT - Universidade de Coimbra

[54] Marques L, Moita F, Nunes U, de Almeida A 1994 3D Laser-Based Sensor for Robotics. In: *Proc. IEEE 7'th Mediterranean Electro. Conf.*, pp 1328–1331

[55] Lee S 1992 Distributed Optical Proximity Sensor System: HexEYE. In: *Proc. IEEE Conf. on Robotics and Automation*, pp 1567–1572

[56] Lee S, Desai J 1995 Implementation and Evaluation of HexEYE: A Distributed Optical Proximity Sensor System. In: *Proc. IEEE Conf. on Robotics and Automation*, pp 2353–2360

[57] Kanade T, Sommer T 1983 An Optical Proximity Sensor for Measuring Surface Position and Orientation for Robot Manipulation. In: *Proc. 3rd International Conference on Robot Vision and Sensory Controls*, pp 667–674



[58] Kanade T, Fuhrman M 1987 A Noncontact Optical Proximity Sensor for Measuring Surface Shape. In: Kanade T (ed), *Three-dimensional machine vision*, Kluwer Academic Publishers, Boston, pp 151–192

[59] Xiong Y, Shafer S A 1993 Depth from Focusing and Defocusing. Tech. Rep. 93-07, The Robotics Institute - Carnegie Mellon University

[60] Nayar S, Watanabe M, Noguchi M Dec 1996 Real-Time Focus Range Sensor. *IEEE Trans Pattern Analysis and Machine Intelligence*, PAMI-18:1186–1198